



**HAL**  
open science

# Multiscale simulation of microcrack nucleation induced by slip localization at the surface of polycrystals

M. Sauzay, J. Liu

► **To cite this version:**

M. Sauzay, J. Liu. Multiscale simulation of microcrack nucleation induced by slip localization at the surface of polycrystals. Journées de Printemps de la SF2M, May 2015, Paris, France. cea-02492570

**HAL Id: cea-02492570**

**<https://cea.hal.science/cea-02492570>**

Submitted on 27 Feb 2020

**HAL** is a multi-disciplinary open access archive for the deposit and dissemination of scientific research documents, whether they are published or not. The documents may come from teaching and research institutions in France or abroad, or from public or private research centers.

L'archive ouverte pluridisciplinaire **HAL**, est destinée au dépôt et à la diffusion de documents scientifiques de niveau recherche, publiés ou non, émanant des établissements d'enseignement et de recherche français ou étrangers, des laboratoires publics ou privés.

# Multiscale simulation of microcrack nucleation induced by slip localization at the surface of polycrystals

Maxime Sauzay<sup>1</sup> and Jia Liu<sup>1,2</sup>

<sup>1</sup>CEA Saclay, DEN/DMN/SRMA, 91191 Gif-sur-Yvette cedex, France

<sup>2</sup>Université Pierre et Marie Curie, 75006 Paris, France

**Abstract.** Crack initiation along surface persistent slip bands (PSBs) has been widely observed and modelled. Nevertheless, from our knowledge, no physically-based fracture modelling has been proposed and validated with respect to the numerous recent experimental data showing the strong relationship between extrusion and microcrack initiation. The whole FE modelling accounts for:

- localized plastic slip in PSBs;
- production and annihilation of vacancies induced by cyclic slip. If temperature is high enough, point defects may diffuse in the surrounding matrix due to large concentration gradients, allowing continuous extrusion growth in agreement with Polak's model. At each cycle, the additional atoms diffusing from the matrix are taken into account by imposing an incremental free dilatation;
- brittle fracture at the interfaces between PSBs and their surrounding matrix which is simulated using cohesive zone modelling.

Any inverse fitting of parameter is avoided. Only experimental single crystal data are used such as hysteresis loops and resistivity values. Two fracture parameters are required: the  $\{111\}$  surface energy which depends on environment and the cleavage stress which is predicted by the universal binding energy relationship.

The predicted extrusion growth curves agree rather well with the experimental data published for copper and the 316L steel. A linear dependence with respect to PSB length, thickness and slip plane angle is predicted in agreement with recent AFM measurement results. Crack initiation simulations predict fairly well the effects of PSB length and environment for copper single and poly- crystals.

## 1 Introduction

Slip localization has been extensively observed in crystals and grains oriented for single slip. Plastic strain is concentrated in thin slip bands which are called persistent slip bands (PSBs) because they reappear at the same positions after intermediate repolishing [1]. Their microstructure is more or less defined depending on slip planarity and therefore on the stacking fault energy of each material [1,2].

Whatever the metallic material, extrusions at the surface of PSBs are generally observed. At low temperature, the extrusion growth stops after a certain number of cycles. This may be explained by the concept of static extrusion (EGMI model [3]). Both production and annihilation of point defects occur during cycling because of dislocation interactions. Once the production and annihilation rates are equal, the concentration of point defects saturates and extrusion growth stops. But, at higher temperature, diffusion from the PSB full of point defects to the surrounding elastic matrix may take place. Even if the PSB concentration of vacancies saturates, additional atoms diffusing from the matrix induce an incremental free dilatation in the PSB at each cycle. The corresponding vacancies migrate in fact towards the matrix and are replaced by matrix atoms. Therefore continuous growth may occur. Such mechanism has been proposed by Polak [4] as an extension of the EGMI model, by considering diffusion as an efficient mechanism even at room temperature for metals like copper. A first analytical solution of the extrusion growth problem has been proposed by Polak and Sauzay [5]. Earlier, Repetto and Ortiz solved numerically a similar problem [6]. Finally, recent atomic force microscopy (AFM) measurements carried out on austenitic stainless steels and ferritic steels show a continuous increase of the extrusion height with respect to the number of cycles, up to at least 30000 cycles [7], which is in agreement with the Polak model prediction [4,5].

Microcrack initiation along the extruded PSBs has been extensively reported in literature, either in single crystals or in polycrystals (see the reviews [1,8]). Very recent SEM observations of cross-

sections obtained by FIB-cuts [8] are in line with the older observations [1]. Therefore, the PSB extrusions, together with the smallest intrusions observed on each PSB side seems to play a role in the microcrack initiation process. This is confirmed theoretically by the computations of Brown and Ogin [9] who showed that a logarithmic stress singularity at the intersections between free surfaces and PSB-matrix interfaces is induced by vacancy dipoles. Such singularity may be induced by the increasing free dilatation due to the production and migration of vacancies as well.

Mura and Tanaka [10] proposed a microcrack initiation criterion based on pile-ups occurring along PSBs. They deduced close-form expressions which have been extensively used in the past. Nevertheless, the major mechanisms described above are not taking into account in their modeling. For instance, the extrusions they modeled would lead to subsurface GB fracture in polycrystals instead of surface crack initiation. More recent developments based on a similar concept can be found in [11]. As slip irreversibility is an important mechanism in cyclic plasticity, the authors of the EGMI model, proposed a complementary model based on slip irreversibility, called EGMI [12]. It allows the statistical computation of the evolution of the surface relief during cycling. Such increasing relief leads to stress concentration and microcrack initiation at the  $N_i^{\text{th}}$  cycle. It is nevertheless not straightforward to deduce close-form expression giving  $N_i$ . And the precise location of microcrack initiation along PSB-matrix interfaces is not predicted by such modelling.

That is why the present work focuses on finite element computations taking into account the most influent mechanisms following old and recent literature: crystal plasticity, slip localization in PSBs, point defect production and migration and finally cohesive zone modelling for simulating the fracture of the PSB-matrix interface. Inverse adjustment of any crystal parameter is excluded from the following work in order to compare extrusion growth and microcrack initiation predictions with numerous observations and data from literature.

## 2 Hypothesis

### 2.1 PSB-matrix microstructure

A single crystal microstructure is considered in the following. The thin slip band of length  $D$  is surrounded by the matrix which is assumed to be elastic (Fig. 1 a). The corresponding slip system is well-oriented (Schmid factor equal to 0.5, Fig. 1 b). Displacements are imposed along the free surface, on the two vertical matrix right and left sides (Fig. 1 a). An assumption of plane strain is made. Rigid body motion is avoided by blocking three well-chosen degrees of freedom. The applied displacement is chosen such that the PSB threshold is reached and the PSB plastic slip is equal to the measured one (respectively 28MPa and 0.0075 for copper at RT [1,2]). The PSB length,  $D$ , thickness,  $t$ , and orientation,  $\alpha$ , (Fig. 1 b) are ones of the main parameters which influence will be discussed in details. A very refined mesh is used along the PSB-matrix interfaces, close to the free surface (Fig. 1 c).

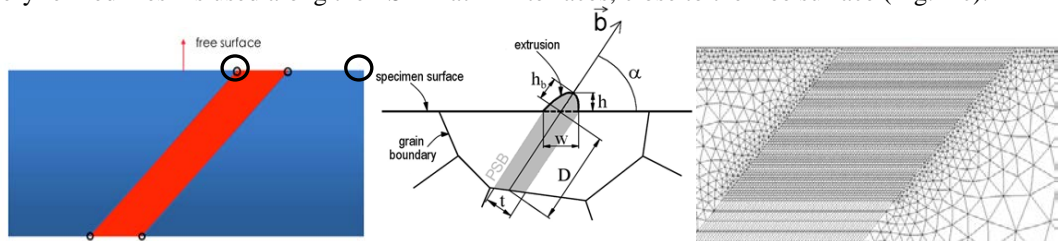


**Figure 1.** a) PSB-matrix microstructure in a single crystal (red PSB, blue matrix, cohesive zone at both interfaces). Stress concentration areas are shown by circles; b) PSB geometry definitions [13]; c) FE mesh of the PSB-matrix microstructure (zoom). Stress concentrations are shown as in Fig. 1 a.

### 2.2 Crystalline elasticity and plasticity laws

Both matrix and PSB obey cubic elasticity, considering either FCC or BCC crystallographic structure. As copper and austenitic stainless steels are the materials considered in the following, the anisotropy of cubic elasticity may not be neglected [14]. Elasticity parameters can be found in [14].

The PSB obeys crystal plasticity as well. Following literature observations, single slip is assumed to occur [1,2]. Isotropic and kinematic hardening display similar amplitudes [15]. The used crystal plasticity laws are described in [15]. The parameters are adjusted using only experimental single crystal hysteresis loop. As the volume fraction of PSBs is known for a given remote plastic strain [1] and the PSB spreads through the whole specimen cross-section, the PSB plastic slip and resolved shear stress are easily deduced from the average single crystal one [1]. At the PSB scale, the adjusted hysteresis loop is shown in Fig. 2 a, together with the one deduced from experiments [16]. For both materials, the predicted threshold value is in agreement with experimental data measured at room temperature: 28MPa (copper, Fig. 2 a) [1,2,16] and 50MPa (316L(N)) [17].

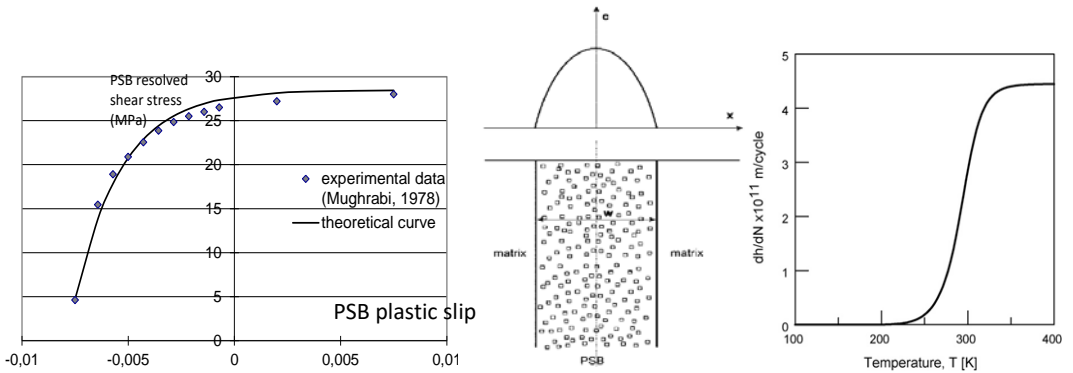


**Figure 2.** a) comparison between the predicted and measured PSB hysteresis loops. Copper, RT; b) production of vacancies in PSBs and induced extrusion. The interfaces at supposed to be perfect sinks (concentration equal to zero) [5]; c) evolution of the extrusion growth rate with respect to temperature, assuming no mechanical interaction between PSB and matrix [5].

### 2.3 Production and annihilation of point defects

The whole sketch is shown in Fig. 2 b. In the following, temperature is assumed to be high enough to get the saturation regime of extrusion growth with respect to temperature. As shown in Figs. 2 c, this regime is almost reached for copper at RT. Then, the increment in volume due to atoms migrating from the matrix to the PSB has been shown to be equal to the production term per cycle,  $p$  [5]. This one has been evaluated based on resistivity measurements carried out on a copper single crystal, just after cycling at 14K [18] and then after an additional annealing time at higher temperature allowing the vanishing of point defects but not of dislocations. In the regime for which no diffusion occurs, the difference in the measured resistivities may be attributed to point defects only. The PSB production rate has been found to be about:  $p=3 \cdot 10^{-7}/\text{cycle}$ .

### 2.4 Cohesive Zone Modelling (CZM)

Such modeling allows the numerical prediction of interface decohesion and microcrack propagation. The CZM constitutive law binds the interface opening displacement and normal stress. Such curve may be qualitatively and even quantitatively deduced from atomistic computations [19]. In the following, three main parameters need to be evaluated:

- the interface elastic Young's and shear moduli which are deduced from the crystal elasticity coefficients and then divided by the interface initial thickness,  $d_0$ . As the fracture along  $\{111\}$  planes is simulated, the initial CZM thickness is assumed to be the inter-atomic distance measured perpendicular to  $\{111\}$  planes:  $d_0=0.21\text{nm}$ ;

- the fracture energy which is equal to two time the free surface of {111} planes. It depends on the material (copper/austenitic stainless steels) and on environment (vacuum/air);
- finally, the maximum stress may be evaluated analytically from the knowledge of the Young modulus, fracture energy and interface thickness. Depending on the shape of the CZM curves, various close-form expressions have been proposed in the past. They differ one from the other by a factor of about two. The universal binding energy relationship (UBER) [20] is used in the following because of its strong atomistic basis.

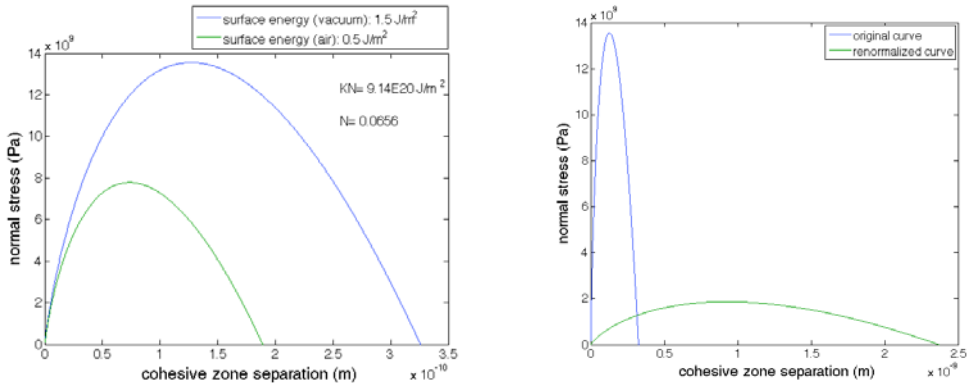


**Figure 3.** a) CZM curves for copper in either vacuum or air (RT); b) original CZM curve plotted with the normalized curve for  $d_{EF}/d_0=54$ , following [20] (vacuum environment).

The CZM parameters for one material and environment are chosen in agreement with data found in literature. Two examples are shown in Fig. 3 a, for copper at room temperature, either in vacuum [21] or in air (surface energy divided by three [10]). Even if the FE size,  $d_{EF}$ , is very small in the stress concentration areas (Figs 1 c), it is nevertheless much larger than the inter-atomic distance,  $d_0$ . Then, the local stress evaluation from the FE computations does not allow us to evaluate normal stress values at a scale consistent with the CZM curve which is valid at the atomistic scale (Fig. 3 a). Nguyen and Ortiz [22] proposed to normalize the CZM curve based on atomistic considerations to get a smoother CZM curve suitable for FE computations using a FE size much higher than  $d_0$ . The normalization uses the ratio between the local FE size and the inter-atomic distance,  $d_{EF}/d_0$ , and is described in details in [20]. The normalized curve is plotted in Fig. 3 b together with the initial CZM curve (Fig. 3 a).

## 2.5 Stability of the results with respect to the numerical parameters

The influence of FE size and time increment have been studied in details. Provided the mesh size close to the microcrack initiation areas (Fig. 1 a) is lower than  $t/90$  (Fig. 1 c), then the relative numerical error on the extrusion height and number of cycles to microcrack initiation is lower than 5%. Microcrack initiation may occur after a few thousand cycles [8] which is out the scope of our computation resources, mainly because of the required strong mesh refinement. That is why one computed cycle mimics a larger number of cycles,  $N_{block}$ . During the computed cycle, an additional free dilatation of  $N_{block}$  time  $p$  is applied whereas the cyclic remote strain is imposed. We make  $N_{block}$  vary from to 3000 down to 250. And we find that provided  $N_{block}$  is lower than, there is no effect of reducing the value of  $N_{block}$ . All the results discussed below are obtained in conditions for which numerical convergence is reached with respect to these numerical parameters.

## 3 Results and comparison with experimental data

### 3.1 Extrusion growth

As expected, the extrusion height increases with the number of cycles (Fig. 4 a). The simulated growth is nevertheless strongly dependent of the slip vector orientation with respect to the tension-compression axis (Fig. 1 b). In case of shearing in the free surface (Burgers vector belonging to the free surface, type A facet following Miller’s definition [23]), the extrusion growth seems rather limited (Fig. 4 a). Its rate is rather low. On the contrary, for type B facets (Figs. 1 a and b), the Burgers vector forms an angle of 45° with respect to the free surface and the predicted growth is much stronger (Fig. 4 a). Therefore, as the slip vector is aligned with the extrusion direction, plastic accommodation seems to make extrusion easier (type B). But if the slip vector is perpendicular to the extrusion direction, plastic accommodation seems much less efficient (type A). These results agree well with the observations and measurements of Obrtlík et al. on copper single crystals [23].

Following Fig. 4 b and Fig. 5 a, the extrusion height depends linearly on the PSB length and thickness respectively. Similar dependences have been highlighted experimentally [13] as shown in Figs. 4 b and Fig. 5 a. In addition, the predicted extrusion heights are in fair agreement with measured values as shown by the comparison between predicted and measured curves provided a similar PSB thickness (Fig. 4 b) or length is used (Fig. 5 a). Finally, FE computations based on meshes built using various PSB angle values,  $\alpha$ , belonging to the range 40-60°, show that the extrusion height is proportional to  $\sin(\alpha)$  as observed by Man et al. experimentally [13]. All the previous parameter studies permits us to deduce a close-form expression allowing the prediction of extrusion height ( $A \approx 3.4 \cdot 10^5 \text{ m}^{-1}$  for copper and  $A \approx 4.5 \cdot 10^5 \text{ m}^{-1}$  for 316L), provided the growth with respect to N is assumed to be linear (low N values):

$$h(N) = ANp \sin(\alpha) tD \tag{1}$$

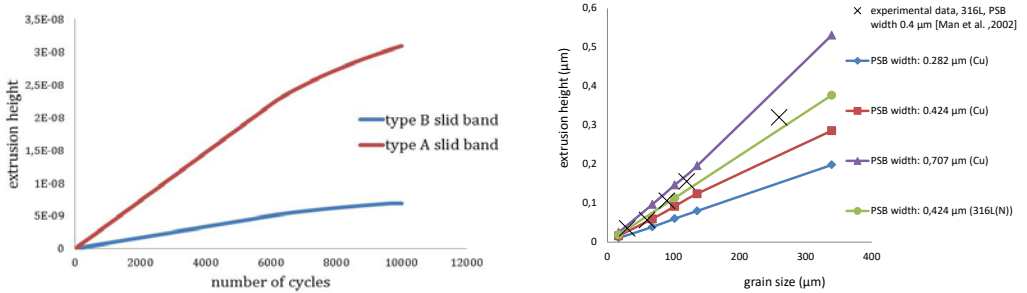


**Figure 4.** a) Evolution of the predicted extrusion height during cycling (type A / type B facets); dependence of the predicted extrusion height after 30000 cycles with respect to grain size and for various PSB widths. Copper & 316L steel. Comparison with experimental data (AFM measurements [13]).

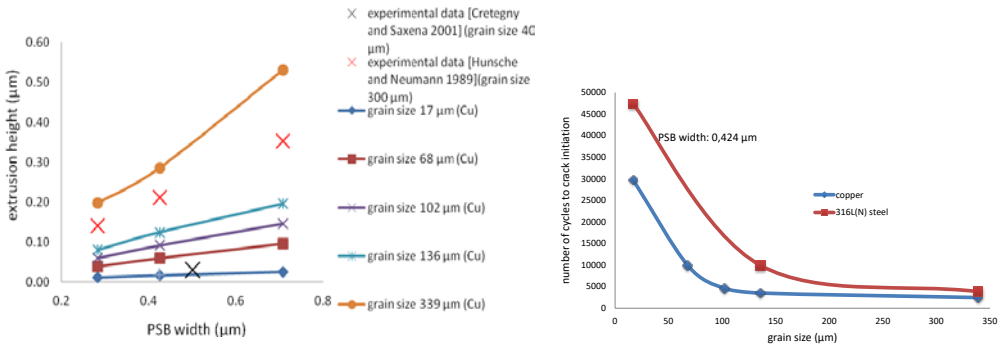


**Figure 5.** a) dependence of the predicted extrusion height after 30000 cycles with respect to PSB width and for various grain sizes, D. Copper. Comparison with experimental data (SEM/AFM measurements); b) Predicted

dependence of the number of cycles to microcrack initiation,  $N_i$ , with respect to  $D$ . Room temperature, air. Free surface energy:  $0.5\text{J/m}^2$  (copper) and  $2.5\text{J/m}^2$  (316L).

### 3.2 Microcrack initiation

Microcrack initiation is defined by the complete opening of the cohesive zone (Fig. 3 b) starting from the free surfaces (Figs. 1 a and c). Whatever the PSB length, thickness and angle, we observe that microcrack initiation takes place as the extrusion height,  $h(N)$ , is equal to a critical value,  $h_c$ . This agrees with many experimental observations [23]. Once more, thanks to numerous parameter studies, a close-form expression may be proposed, allowing the prediction of the critical height,  $h_c$ , and number of cycles to microcrack initiation,  $N_i$ , depending on microstructure features and environment.

$$h_c = Bt\sqrt{\gamma_s} \quad (2)$$

With  $B \approx 0.034 \text{ J}^{-1/2}\text{m}$  for copper. Equating the first terms of Eqs. (1) and (2) leads to:

$$N_i = C \frac{\sqrt{\gamma_s}}{\rho D \sin(\alpha)} \quad (3)$$

with  $C = B/A \approx 1.0 \cdot 10^{-7} \text{ J}^{-1/2}\text{m}^2$  for copper ( $C \approx 1.58 \cdot 10^{-7} \text{ J}^{-1/2}\text{m}^2$  for 316L steel). This analytical expression is in fair agreement with the numbers of cycles computed by the FE method (plotted in Fig. 5 b). The higher the grain size, the lower the required number of cycles to microcrack initiation, in agreement with experimental observations [24].

The predicted and measured  $N_i$  values are given in Table 1, for 316L steel and copper at RT, in air or vacuum, and either for single or poly- crystals. For both materials, the predicted and measured numbers of cycles to microcrack initiation differ by less than a factor 2.5 which is encouraging as no inverse parameter fitting has been used. For 316L steel, the computed  $N_i$  may be overestimated, partly because intrusions are not taken into account in the previous computations whereas they seem to play a role in microcrack initiation following the recent observations of Man et al. [25].

**Table 1.** Comparison between the computed and experimental numbers of cycles to microcrack initiation,  $N_i$ . Tension-compression except for the experiments of Tanaka et al., 2006 (reversed, torsion, total shear stress amplitude: 0.35%), room temperature,  $\alpha = 45^\circ$ . For single crystals, the PSB length,  $D$ , is equal to the specimen thickness times  $\sin(\alpha)$ . For polycrystals, the length measured by the intercept line method is multiplied by 1.5 to get the circle diameter.

material	Environment	t (μm)	D (μm)	$E_p$ or $\Sigma$ (MPa)	$\gamma_s$ [21,10] $\text{J/m}^2$	$N_i$ (meas.)	$N_i$ (cal.)	Ref. (experiment)
Cu, polycrystal	air	0.5	360	$10^{-4}$ $-5.8 \cdot 10^{-4}$	0.6	100-1000	1050	Kwon et al., 1989
Cu, polycrystal	vacuum	0.5	360	$1.3 \cdot 10^{-4}$	1.95	5000-10000	2060	Kwon et al., 1989
Cu, polycrystal	air	0.5	~100	$5.8 \cdot 10^{-4}$	0.6	>100 <3500	3700	Kim et al. 1991
Cu, single crystal	air	1-1.8	3500	$1.2 \cdot 10^{-4}$ $-10^{-3}$	0.6	200-500	111	Kwon et al., 1989
Cu, single crystal	vacuum	1-1.8	3500	$10^{-3}$	1.95	500-1000	190	Kwon et al., 1989
316L, polycrystal	air	0.5	60	$10^{-3}$	0.8	>1800 <3800	10090	Polak et al., 2009
316L, polycrystal	air	0.5	80	~ $10^{-3}$	0.8	>500	8160	Polak et al., 2013
316L, polycrystal	air	0.5	160	250	0.8	3500-10000	5060	Tanaka et al., 2006

## References

1. Z.S. Basinski, S. J. Basinski, Prog. Mater. Sci., **36** 89 (1992)
2. M. Sauzay, L.P. Kubin, Prog. Mater. Science, **56** 725 (2011)
3. U. Essmann, U. Gösele, H. Mughrabi, Phil. Mag. A **44** 405(1981)
4. J. Polak, Mat. Sci. Eng. **92** 71 (1987)
5. J. Polak, M. Sauzay, Mat. Sci. Eng. A **500** 122 (2009)
6. E.A. Repetto, M. Ortiz, Acta Mater. **45** 2577 (1997)
7. J. Man, K. Obrtlík, J. Polak, Phil. Mag. **89** 1337 (2009)
8. J. Man, K. Obrtlík, J. Polak, Phil. Mag. **89** 1295 (2009)
9. L.M. Brown, S.L. Ogin, *Fundamentals in deformation and fracture*, 501, B.A. Bilby, K.J. Miller, J.R. Willis (Eds.) (Cambridge University Press, Cambridge, 1985)
10. G. Venkataraman, Y.-W. Chung, Y. Nakasone, T. Mura, Acta Metall. Mater. **38** (1990)
11. M.D. Sangid, H.J. Maier, H. Sehitoglu, Int. J. Plast. **27** 801 (2011)
12. K. Differt, U. Essmann, H. Mughrabi, Phil. Mag. A **54** 237 (1986)
13. J. Man, K. Obrtlík, C. Blochwitz, J. Polak, Acta Mater. **50** (2002) 3767 -3780.
14. M. Sauzay, Acta. Mater. **55** 1193 (2007)
15. A. Steckmeyer, M. Sauzay, A. Weidner, E. Hieckmann, Int. J. Fat. **40** 154 (2012)
16. H. Mughrabi, Mat. Sci. Eng. **33** 207 (1978)
17. C. Gorlier. Mécanismes de fatigue plastique de l'acier 316L sous formes monocristalline et polycristalline. Thèse Ecole des Mines de Saint Etienne (1984).
18. Z.S. Basinski , S.J. Basinski, Acta Metall. **37** 3255 (1989)
19. V. Yamakov, E. Saether, D.R. Phillips, E.H. Glaessgen, J. Mech. Phys. Sol. **54** 1899 (2006)
20. O. Nguyen, M. Ortiz, J. Mech. Phys. Sol. **50** 1727 (2002)
21. M.C. Inman, D. McLean, H.R.Tipler. Proc. Roy. Soc. A273 538 (1963)
22. K. Obrtlík, J. Man, J. Polak, Mat. Sci. Eng. A **234-236** (1997) 727-730.
23. M. Risbet, X. Feaugas, Eng. Fract. Mech. **75** 3511 (2008)
24. H.S. Ho, M. Risbet, X. Feaugas, J. Favregeon, G. Moulin, Proced. Eng. **2** 751 (2010)
25. J J. Man, T. Vystavel, A. Weidner, I. Kubena, M. Petrevec, T. Kruml, J. Polak, Int. J. Fat. **39** 44 (2002)

Remerciements: les auteurs remercient l'Institut de Radioprotection de Sûreté Nucléaire (IRSN) pour leur soutien technique.